ACS APPLIED MATERIALS & INTERFACES

Research Article

www.acsami.org

Enhanced Removal of Methylene Blue and Methyl Violet Dyes from Aqueous Solution Using a Nanocomposite of Hydrolyzed Polyacrylamide Grafted Xanthan Gum and Incorporated Nanosilica

Soumitra Ghorai,[†] Asish Sarkar,[†] Mohammad Raoufi,[‡] Asit Baran Panda,*[,§] Holger Schönherr,*[,‡] and Sagar Pal*[,†]

[†]Polymer Chemistry Laboratory, Department of Applied Chemistry, Indian School of Mines, Dhanbad 826004, India

[‡]Physical Chemistry I, Department of Chemistry and Biology, University of Siegen, 57076 Siegen, Germany

[§]Disciplines of Inorganic Materials and Catalysis, Central Salt and Marine Chemicals Research Institute (CSIR-CSMCRI), Bhavnagar 364021, India

Supporting Information

ABSTRACT: The synthesis and characterization of a novel nanocomposite is reported that was developed as an efficient adsorbent for the removal of toxic methylene blue (MB) and methyl violet (MV) from aqueous solution. The nanocomposite comprises hydrolyzed polyacrylamide grafted onto xanthan gum as well as incorporated nanosilica. The synthesis exploits the saponification of the grafted polyacrylamide and the in situ formation of nanoscale SiO_2 by a sol−gel reaction, in which the biopolymer matrix promotes the silica polymerization and therefore acts as a novel template for nanosilica formation. The detailed investigation of the kinetics and the adsorption isotherms of MB and MV from aqueous solution showed that the dyes adsorb rapidly, in accordance with a pseudo-second-order kinetics and a Langmuir adsorption isotherm. The entropy driven process was furthermore found to strongly depend on the point of zero charge (*pzc*) of the adsorbent. The remarkably high adsorption capacity of dyes on the nanocomposites (efficiency of MB removal, 99.4%; maximum specific removal Q_{max}, 497.5 mg g^{-1}; and efficiency of MV removal, 99.1%; Q_{max}, 378.8 mg g^{-1}) is rationalized on the basis of H-bonding interactions as well as dipole−dipole and electrostatic interactions between anionic adsorbent and cationic dye molecules. Because of the excellent regeneration capacity the nanocomposites are considered interesting materials for the uptake of, for instance, toxic dyes from wastewater.

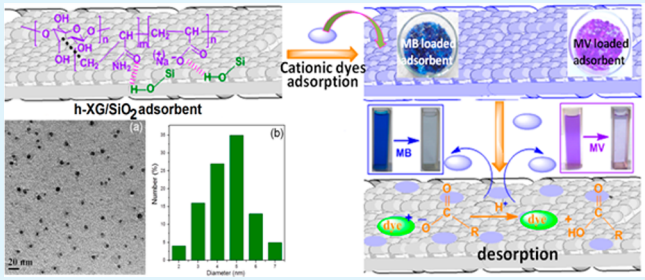

KEYWORDS: *xanthan gum, nanocomposite, adsorption, dye removal, methylene blue, methyl violet*

1. INTRODUCTION

Water pollution with toxic dyes, metal ions and organic contaminants constitutes a serious environmental hazard in particular for aquatic biosystems, where symbiotic processes may be affected, e.g., by reducing the photosynthetic activity.[1] Thus, the efficient decontamination of dye pollutants via reliable and ecofriendly techniques has garnered considerable attention recently.[2] Among the various chemical, physical, and biological treatment processes, adsorption is a simple, yet effective method for dye uptake.[3,4]

Both methylene blue (MB) and methyl violet (MV) are typical examples of industrially relevant toxic cationic dyes with known harmful effects on humans.[5−8] From a toxicological as well as from an ecological point of view it is therefore essential to treat effluents containing these and related dyes.

It is well-established that various adsorbents including polymers are widely used for the remediation of effluents in the dye industry.[9−13] Among those, ready available naturally occurring polymers, such as polysaccharides, are potentially applicable as adsorbents because they are low-cost, non-toxic, and eco-friendly in nature.[13] However, until now, the use of polysaccharides as adsorbents was limited due to their poor specific surface area, comparatively low hydrodynamic volume and limited potential to form H-bonding with dyes because of extensive intramolecular chain interactions.[13] To overcome these shortcomings, many efforts have been undertaken recently to develop modified biopolymer-based adsorbents in order to introduce the combined functionality of both constituents.[14,15]A promising strategy is to graft long, flexible synthetic polymer chains onto the polysaccharide backbone.[16] However, simple non-ionic graft copolymers may have certain limitations like the lack of electrostatic interactions with ionic dyes. Therefore, the development of adsorbents, which carry permanent charges, on the basis of graft copolymers of

Received: December 4, 2013
Accepted: March 3, 2014
Published: March 3, 2014

   dx.doi.org/10.1021/am4055657 | ACS Appl. Mater. Interfaces 2014, 6, 4766−4777

polysaccharides is a worthwhile target to improve the adsorption efficiency.

For an efficient adsorption process a high adsorption capacity Q_{max} of the adsorbent as well as a good regeneration capacity is of paramount importance.[2,3,10,17] More recently, nanocomposites were reported to possess many advantages in this respect, which are linked to their high surface area, increased number of active sites, high thermal stability and polyfunctional characteristics.[18,19] In particular well-defined, monodisperse silica nanoparticles have garnered attention also because they render flexible surface modification feasible.[20,21] In addition, polysaccharides were shown to act as a template for the in situ silica generation[22] and growth through interactions between several −OH groups present in polysaccharides with the silica surface.[22−24] Therefore, the in situ synthesis of templated modified polysaccharide/silica materials obtained via the sol-gel technique may open new pathways for the formation of hybrid nanocomposites.[22−25]Compared to modified polysaccharides, such nanocomposites promise to yield improved porosity, better surface area and hydrodynamic radius, and enhanced mechanical resistance.[22−25]

Recently modified polysaccharides (such as xanthan gum[24] and carboxymethyl tamarind[26]) and silica based nanocomposites have been developed in our laboratories as adsorbents for the uptake of toxic Pb (II)[24] and Congo red dye[21] as well as for use as flocculant.[27] Despite its useful properties, the reported modified xanthan-based composite materials[24] are non-ionic in nature and therefore not optimal for the elimination of cationic dyes. In contrast, modified carboxymethyl tamarind-based nanocomposites,[26] although anionic in nature, were found to be less capable for the separation of MB from aqueous solution (Q_{max} = 43.85 mg g^{-1} after 120 min).[26] This behavior can be in parts attributed to the ex situ incorporation of commercial nanosilica into the copolymer matrix.

In this paper we report on the development, characterization and application of novel nanocomposites derived from hydrolyzed polyacrylamide grafted xanthan gum and its nanosilica composite (h-XG/SiO_2) through a sol-gel method as adsorbents to remove both MB and MV from aqueous solution. The partial hydrolysis of polyacrylamide chains grafted onto xanthan gum affords electrostatic charges that result in an increased hydrodynamic volume[5] and enhanced electrostatic attraction with cationic dyes, resulting in a significantly higher adsorption efficiency. The nanocomposites obtained show rapid adsorption and excellent adsorption efficiencies for uptake of both MB and MV from aqueous solution, which improves the performance beyond the state of the art reported in the literature.[2,3,6−8,13,15,17,26,28−37]

2. EXPERIMENTAL SECTION

2.1. Chemicals. XG-g-PAM was used as synthesized earlier.[24] Tetraethylorthosilicate (98%, TEOS, Sigma-Aldrich, USA), ammonium hydroxide (30%, NH_3, Merck, India), sodium hydroxide (Merck, India) and ethanol (99.9% pure, Merck, India) and the dyes MB (λ_{max}, 662 nm, Loba Chemie Pvt. Ltd., Mumbai, India) and MV (λ_{max}, 585 nm, Loba Chemie Pvt. Ltd., Mumbai, India) were of analytical grade. Double distilled water was used for all experiments.

2.2. Synthesis of h-XG and Nanocomposites (h-XG/SiO_2). For the alkaline hydrolysis reaction, 1 g graft copolymer (i.e. XG-g-PAM)[24] was dissolved in 100 mL double distilled water and under stirring the required amount of 0.1 (N) NaOH solution was added to the mixture (details, Table 1). At the end of the required reaction time (compare Table 1), the mixture was cooled to room temperature and washed with 400 mL of ethanol. Finally, the product was dried in a vacuum oven at 60°C. Different h-XGs were prepared by altering the reaction conditions to optimize the material having a lower neutralization equivalent and a higher intrinsic viscosity.

Table 1. Synthesis Details of the Hydrolyzed Polyacrylamide Grafted Xanthan Gum (h-XG) and in Situ Silica Incorporated Hydrolyzed Polyacrylamide Grafted Xanthan Gum (h-XG/SiO_2)

polymer	amount of 0.1 (N) NaOH (mL)	reaction time (h)	reaction temperature (°C)	neutralization equivalent (g)	intrinsic viscosity (dL/g)
h-XG 1	25	2	60	3142.8	43.7
h-XG 2	50	2	60	1245.6	46.8
h-XG 3	75	2	60	7142.7	41.1
h-XG 4	50	3	60	1038.1	48.0
h-XG 5	50	4	60	657.2	54.2
h-XG 6	50	5	60	905.2	51.7
h-XG 7	**50**	**4**	**70**	**416.4**	**59.5**
h-XG 8	50	4	80	537.3	56.0

polymer	amount of TEOS (mL)	amount of EtOH, 12 (N) NH_4OH, and time	intrinsic viscosity (dL/g)
h-XG/SiO_2 1	2		67.8
h-XG/SiO_2 2	**2.5**	4 mL, 2 mL, 12 h	**74.2**
h-XG/SiO_2 3	3		70.8

The nanocomposites were synthesized in situ by adding the required amount of TEOS (dissolved in 4 mL of ethanol) and subsequently 12(N) ammonium hydroxide solution to the aqueous solution of the h-XG. The reaction was carried out under stirring (400 rpm) at 70°C for 4 h. Finally, the nanocomposite was precipitated by adding 250 mL of acetone and followed by drying in a vacuum oven at 50 °C, grounding and finally sieving through a 125 μm sieve.

2.3. Determination of the Neutralization Equivalent (NE) of h-XG. The neutralization equivalent (NE) is the equivalent weight of an acid for neutralization, which was calculated by titration with a standard base.[38] The NE of h-XG was measured (Table 1) as reported earlier.[38,39]

2.4. Characterization. Intrinsic viscosities were measured with an Ubbelohde Viscometer in 0.1 M sodium nitrate solution at 25 °C. The elemental analyses were performed with a Perkin Elmer Elemental Analyzer (Series-II, CHNS/O Analyzer-2400). ^{13}C and ^{29}Si magic angle spinning (MAS) nuclear magnetic resonance (NMR) spectra were recorded in the solid state using a 500 MHz Bruker Advance II-500NMR spectrometer. FTIR spectra were recorded in solid state (KBr pellet method) using a Model Spectrum 2000 FTIR spectrometer (Perkin Elmer). The thermal analysis of h-XG and the h-XG/SiO_2 nanocomposite was carried out using a thermo gravimetric analyzer (TGA Q 500, TA, USA) with a heating rate of 5°C/min in a nitrogen atmosphere.The surfaces of h-XG and the h-XG/SiO_2 nanocomposites were analyzed using field emission scanning electron microscopy (Zeiss Ultra 55cv FESEM, Zeiss, Germany) and transmission electron microscopy (Model: JEM 2100, JEOL, Japan). Additional energy-dispersive X-ray (EDAX) analysis was carried out in a field emission SEM (Model − FESEM Supra 55, Zeiss, Germany). The specific surface area, total pore volume and pore size distribution analyses were performed using a NOVA 3200e instrument (Quantachrome, USA). The details of the measurement procedures were reported earlier.[21] The zeta potential was measured using a Zetasizer Nano-ZS90 (Malvern, UK). The rheological characteristics of various h-XGs and nanocomposites were investigated using a Paar Physica Advanced Rheometer.

2.5. Adsorption Studies. The dye uptake study was performed using an orbital shaker (Rivotek, Kolkata, India). In particular, the effect of altered solution pH, temperature, contact time, initial dye

dx.doi.org/10.1021/am4055657 | ACS Appl. Mater. Interfaces 2014, 6, 4766−4777

concentration and adsorbent dosage were analyzed according to previously reported procedures.[21] For all the uptake study, 25 mL of dye solution was used. The % of dye adsorption was calculated using eq 1[21]

$$\% \text{ adsorption} = \frac{C_0 - C_e}{C_0} \times 100 \quad (1)$$

The equilibrium uptake was calculated using eq 2[21,24]

$$q_e = (C_0 - C_e) \times \frac{V}{W} \quad (2)$$

Where q_e represents equilibrium capacity of dye on nanocomposite (mg. g^{-1}), C_0 and C_e are the initial and equilibrium concentrations of adsorbate solution (mg L^{-1}), respectively. V denotes the volume of the dye solution used (L) and W is the weight of the adsorbent (g) used.[21] The results shown here are the arithmetic mean of three readings.

2.6. Desorption Study. The regeneration ability of the nanocomposites was determined in four subsequent adsorption-desorption cycles. The desorption experiment was performed in the same way as reported before,[21] however, stripping solutions with a pH of 2, 7, and 10 were used to evaluate the maximum regeneration efficacy of dye (with 25 mL of 400 ppm MB solution mixed with 30 mg of h-XG/SiO_2 nanocomposite for 20 min at 323 K. For MV, the desorption conditions were: dye concentration, 350 ppm; adsorbent dosage, 40 mg/25 mL; contact time, 15 min; and temperature, 313 K). The % desorption was calculated with eq 3[40]

$$\% \text{ desorption} = \frac{\text{concentration desorbed (mg/L)}}{\text{concentration adsorbed (mg/L)}} \times 100 \quad (3)$$

3. RESULTS AND DISCUSSION

3.1. Synthesis. *3.1.1. Synthesis of Hydrolyzed Xanthan Gum (h-XG).* The alkaline hydrolysis reaction of XG-g-PAM[24] affords stiffened and straightened graft copolymer chains, since the adjacent negatively charged carboxylic acid groups formed by the conversion of $-CONH_2$ groups will repel each other.[39] Known side reactions are the deetherification and depolymerization. Khalil et al. pointed out that the desired conversion of amide to carboxylic groups increases with NaOH concentration up to 0.1 (M) NaOH.[41] For higher concentrations, the side reactions compete significantly.[38] As expected, the NE values of partially hydrolyzed XG were found to depend on the NaOH concentration along with the time and temperature of the reaction.[39] h-XG 7 was shown to possess the lowest NE value of 416.4 (Table 1), i.e., the highest number of carboxylate groups, which is considered an optimum for the adsorption of dyes (vide infra).

3.1.2. Synthesis of the Nanocomposite (h-XG/SiO_2). h-XG/SiO_2 hybrid nanocomposites form according to the established sequences of (i) the initial hydrolysis of TEOS, (ii) the condensation of silanol groups to afford oligomers assembled as sol particles and finally (iii) the cross linking of sol particles to a sol−gel transition. The precursor medium accelerates the sol-gel process in the presence of h-XG. Here, h-XG acts as a template for the nucleation and growth of a SiO_2 shell because of the H-bonding between the $-COO^-$/$-CONH_2$ groups of the surface of modified XG and hydroxyl groups at the SiO_2 nanoparticle surface, as shown in Scheme 1. In presence of h-XG, the silanol groups can further be hydrolyzed and contribute in the polycondensation reaction[25] to generate nano scale silica in the polymer matrix.

3.2. Characterization. The value of the intrinsic viscosity of different grades of h-XG is much higher than that of the XG-g-PAM,[24] as shown in Table 1. Due to the alkaline hydrolysis of the grafted PAM chains, the repulsive forces between adjacent

Scheme 1. Schematic for the Synthesis of h-XG/SiO_2 Nanocomposites

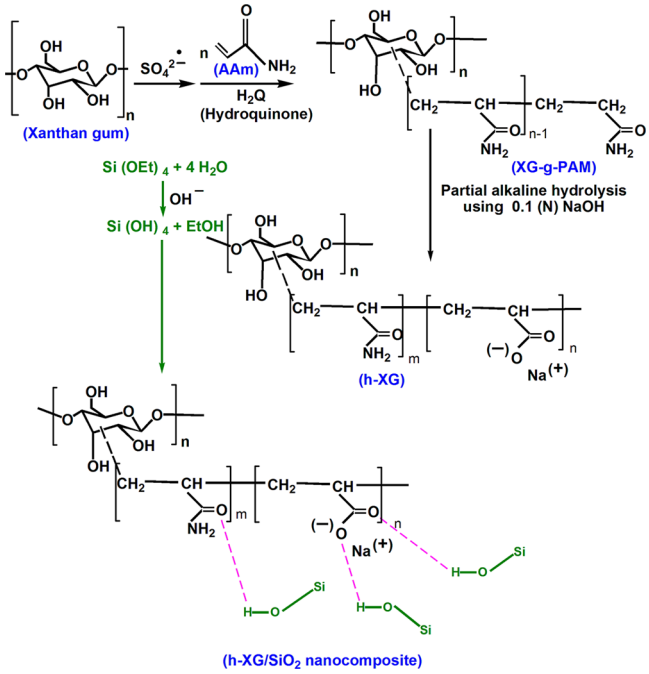

$-COO^-$ groups formed in the hydrolysis are enhanced and straighten the flexible chains. Therefore, the hydrodynamic volume and in turn the intrinsic viscosity of h-XG solutions increased. For h-XG 7 the electrostatic repulsion was maximal, resulting in a higher hydrodynamic volume, because of the maximum content of carboxylate groups (i.e., lower NE Value). The intrinsic viscosity of the h-XG/SiO_2 nanocomposites increased drastically in comparison to h-XG because of the H-bonding interaction between the active sites of the modified polysaccharide and the silanol groups. h-XG/SiO_2-2 showed the highest intrinsic viscosity values, presumably because of the unique and better distribution of silica nanoparticles.

The conversion of $-CONH_2$ groups during the alkaline hydrolysis was verified by elemental analyses, which showed a lower % of N and a higher % of O (see Table S1 in the Supporting Information). Further, for nanocomposite h-XG/SiO_2-2, the silanol groups at the surface of the h-XG matrix increased the % of O in the composite product (see Table S1 in the Supporting Information).

The solid-state ^{13}C NMR spectrum of h-XG7 (Figure 1a) revealed all the characteristics peaks of xanthan gum as well as those for polyacrylamide[24] (see Table S2 in the Supporting Information). However, the presence of an additional peak at δ = 169.2 ppm signifies the presence of the carbon atom of the carboxylate groups (see Table S2 in the Supporting Information), which are absent in XG-g-PAM.[24] This signal supports the occurrence of the saponification reaction during the alkaline hydrolysis of the grafted chains, as shown in Scheme 1. Further, the spectra of all nanocomposites (Figure 1b−d) exhibited a regular downfield shift of the NMR peaks attributed to the amide, carboxylate and $-CH_2OH$ groups (see Table S2 in the Supporting Information), presumably because of the interaction between h-XG and silanol groups. h-XG/SiO_2-2 (Figure 1c) evidenced a greater shift of both amide and carboxylate groups (see Table S2 in the Supporting Information), probably due to the improved distribution as

dx.doi.org/10.1021/am4055657 | ACS Appl. Mater. Interfaces 2014, 6, 4766−4777

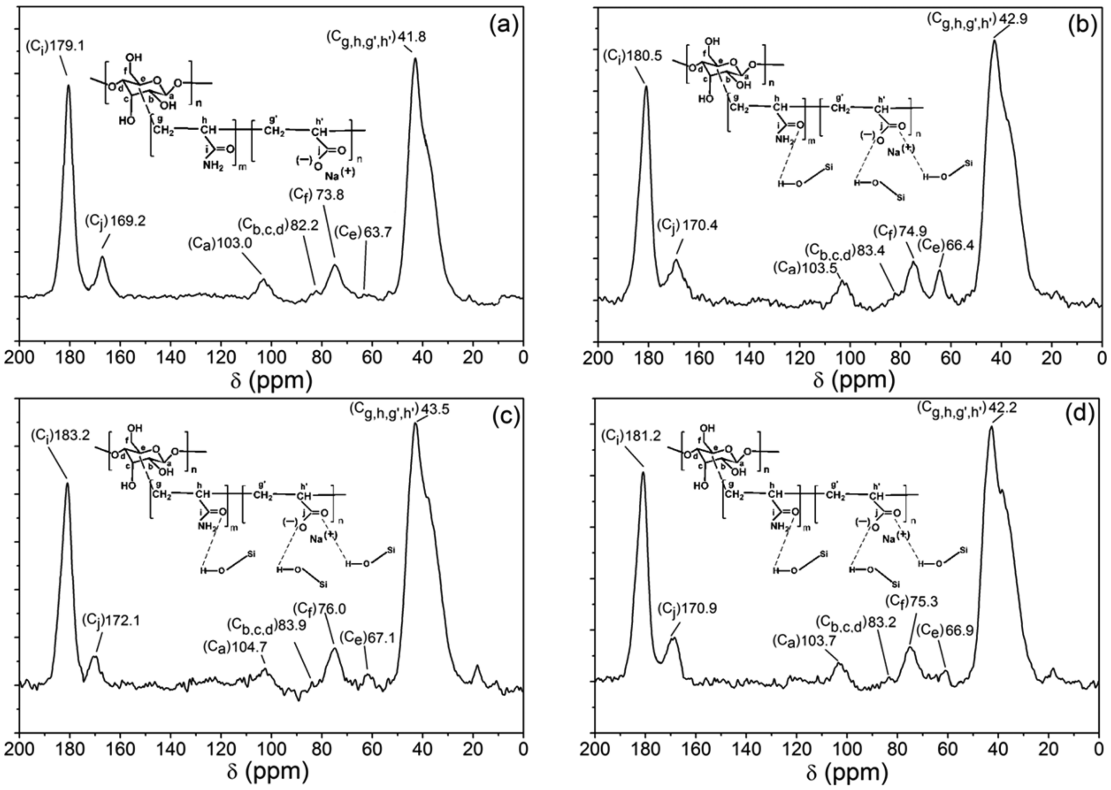

Figure 1. ^{13}C NMR spectra of (a) h-XG 7, (b) h-XG/SiO_2-1, (c) h-XG/SiO_2-2, (d) h-XG/SiO_2-3.

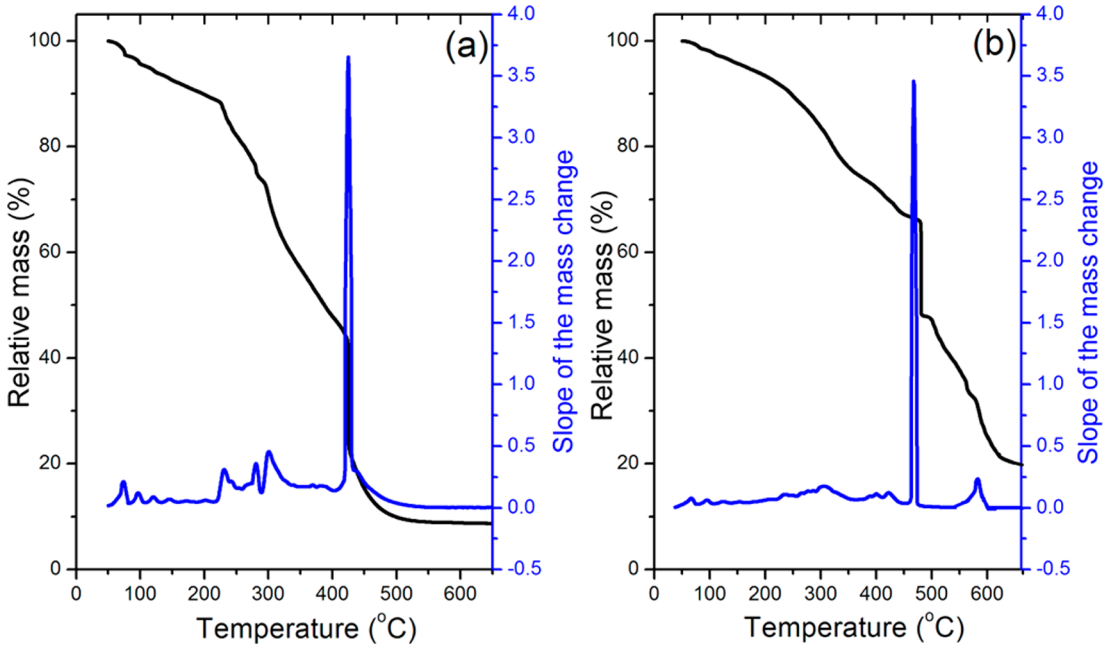

Figure 2. TGA thermograms of (a) h-XG 7, and (b) h-XG/SiO_2-2.

well as the better interaction of h-XG with the in situ formed silica nanoparticles.

The solid state ^{29}Si MAS NMR spectrum of the h-XG/SiO_2-2 (see Figure S1 in the Supporting Information) was found to be near identical to the spectrum of Stöber silica,[24] which supports the incorporation of silica in the nanocomposite. However, in comparison to Stöber silica,[24] the spectrum of h-XG/SiO_2-2 was noisier, possibly because of the existence of a significant amount of carbon in h-XG.

The presence of silica particles in the composites was also confirmed by EDAX analysis (see Figure S2 in the Supporting Information).

Figure 2 elucidates the results of the comparative TGA and DTG analysis of h-XG 7 and the h-XG/SiO_2-2 nanocomposite. The TGA curve of h-XG 7 (Figure 2a) shows four regions of mass loss. The initial mass loss (between 50 and 100 °C) may be attributed to the loss of moisture present in the material. The second mass loss (between 220 and 300 °C) can be

dx.doi.org/10.1021/am4055657 | ACS Appl. Mater. Interfaces 2014, 6, 4766−4777

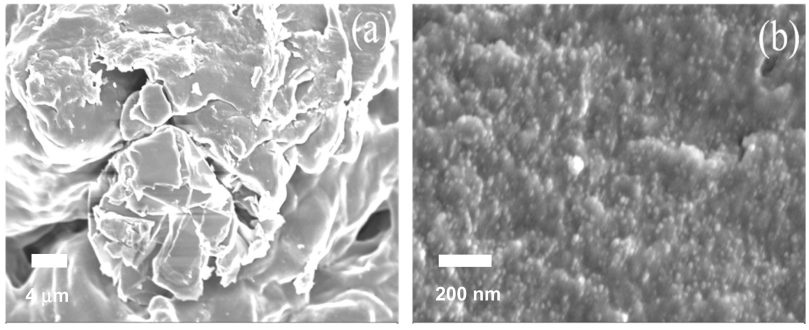

Figure 3. FESEM micrographs of (a) h-XG 7, and (b) h-XG/SiO_2-2.

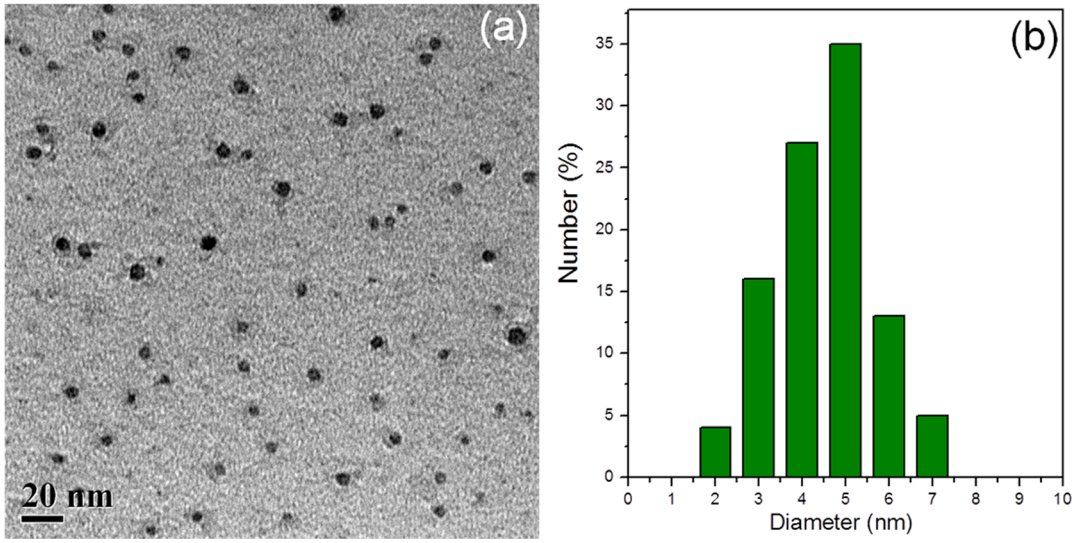

Figure 4. (a) TEM image and (b) particle size distribution of nanocomposite h-XG/SiO_2-2 as determined by TEM.

assigned to the decomposition of the polysaccharide backbone,[27] while the third zone of mass loss (between 310 and 400°C) suggests the elimination of NH_3 from the grafted polyacrylamide chains.[27] Finally, between 450 and 500°C, CO_2 may be eliminated from the h-XG backbone. By contrast, the thermogram of the h-XG/SiO_2-2 nanocomposite (Figure 2b) exhibits an additional region of mass loss (560 and 670 °C). This mass loss is tentatively attributed to the degradation of the silanol −OH groups present in the silica surface,[42] which supports the successful assimilation of silica particles on h-XG.

The FE-SEM micrograph of h-XG 7 (Figure 3a) shows an interconnected three-dimensional network with a porous structure. The FE-SEM image of the nanocomposite h-XG/SiO_2-2 (Figure 3b) unveils that smaller, spherical silica nanoparticles (discernible as circular features with pronounced secondary electron emission) are well-embedded and homogeneously distributed throughout the porous surface of the h-XG matrix. This suggests that SiO_2 nanoparticles are attached to the surface of h-XG, because of the H-bonding interaction between the silanol groups and the active sites of polymer matrix.

The TEM image (Figure 4a) of nanocomposite h-XG/SiO_2-2 shows a uniform distribution of spherical silica particles with diameters ranging from 2 to 7 nm throughout the polymer matrix (compare also the histogram of the particle size distribution, Figure 4b). In addition, it has also been observed that the silica particles were well dispersed for h-XG/SiO_2-1 (see Figure S3a in the Supporting Information) and h-XG/SiO_2-3 (see Figure S3b in the Supporting Information). For comparison, Figure S4 (see the Supporting Information) shows a TEM image of neat Stöber silica, in which the silica particles apparently agglomerated. The observation of isolated nanoparticles in the nanocomposites is consistent with the template effect of hydrolyzed XG during the in situ synthesis (vide supra). Thus, we assume that the polymer chains of h-XG act as a promoter for the nucleation and growth of the silica nanoparticles in the system as well as a stabilizer. In nanocomposite h-XG/SiO_2-2 (Figure 4), the nanoparticles were very homogeneously distributed in the modified polysaccharide, probably because of the better matrix−filler interaction.

The incorporation of silica nanoparticles in the h-XG 7 through in situ synthesis results in a considerable increase in the surface area in comparison to h-XG 7. This was unveiled by surface area and pore structure determinations of h-XG 7 and h-XG/SiO_2-2 using the nitrogen isothermal adsorption technique (Table 2). Figure S5 (see the Supporting Information) shows N_2 adsorption−desorption isotherms and pore size distributions of h-XG7 and the nanocomposite h-XG/

Table 2. Surface Parameters of h-XG 7 and h-XG/SiO_2-2 Nanocomposites

sample	BET surface area (m^2 g^{-1})	BJH pore volume (cm^3 g^{-1})	pore size (Å)
h-XG 7	34.3	0.56	35.6
h-XG/SiO_2-2	398.0	0.67	40.6

dx.doi.org/10.1021/am4055657 | ACS Appl. Mater. Interfaces 2014, 6, 4766−4777

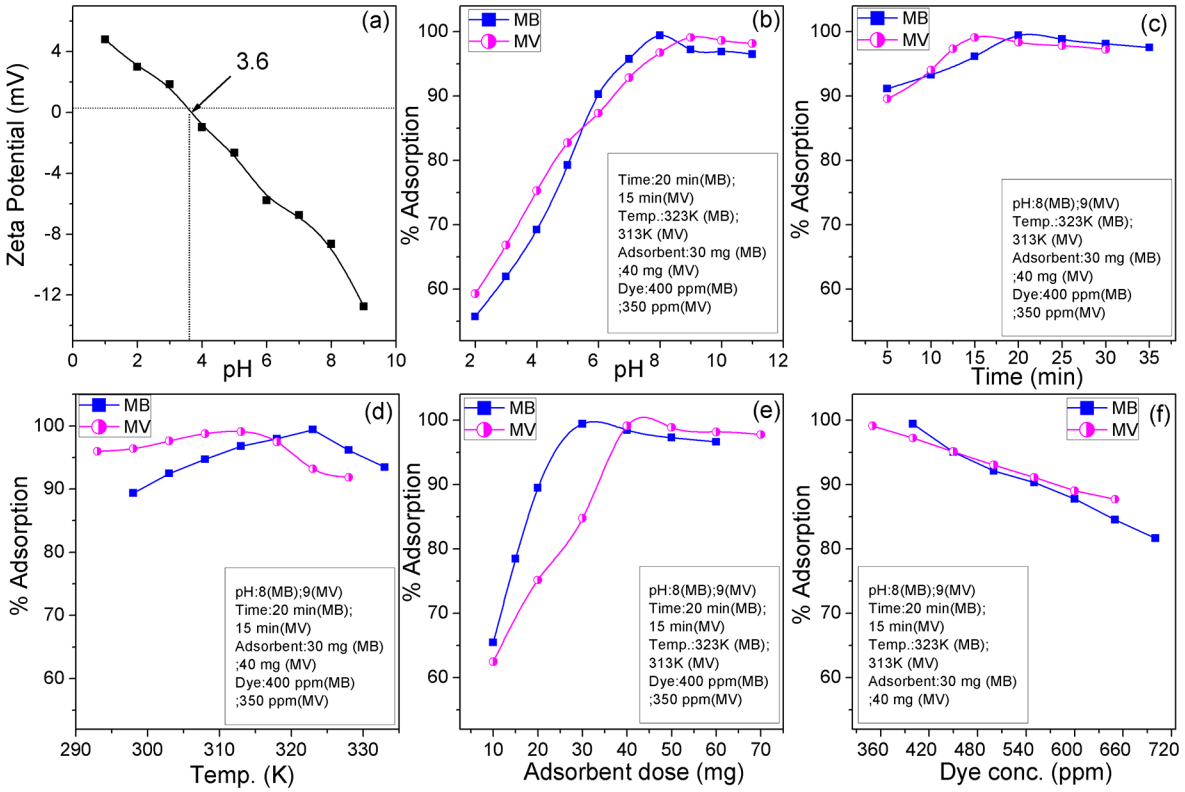

Figure 5. (a) Effect of pH on zeta potential of h-XG/SiO_2-2 nanocomposite and effect of (b) pH, (c) time, (d) temperature, (e) adsorbent dosage, and (f) initial dye concentration on adsorption characteristics of MB and MV from aqueous solution using the h-XG/SiO_2-2 nanocomposite.

SiO_2-2. It is evident that the interfacial interactions between the templated h-XG copolymer matrix and the silica nanofiller greatly affect the materials' pore structure.[43]

All the materials investigated show a typical shear thinning behavior (see Figure S6 in the Supporting Information). h-XG 7 showed the highest shear viscosity among the hydrolyzed xanthan gums, probably owing to the stronger electrostatic repulsion between the carboxylate groups present in this composition (h-XG 7 showed the lowest NE value). Clearly, all the nanocomposites exhibited higher shear viscosities than the neat hydrolyzed product. This may be due to the fact that the nanocomposites are hetero phase materials and because of the polymer matrix-nanosilica interactions, there is an increase in solution viscosity. Nevertheless, h-XG/SiO_2-2 exhibited the highest viscosity, because of the enhanced interaction of the h-XG and the filler, which originates from the homogeneous distribution of the SiO_2 particles.

3.3. Adsorption Characteristics. *3.3.1. Optimization of the Adsorption Conditions of Cationic Dyes.* Removal of toxic dyes from aqueous solution using an adsorbent is well known to depend on temperature, the solution pH, added salt, the equilibrium time of adsorption, the adsorbent dosage and finally the initial concentration of the dye.[21]

Effect of pH. Figure 5b demonstrates that a maximum % of color removal was observed at pH 8 for MB (99.4 %) and at pH 9 for MV (99.1 %), beyond which it was constant. To determine the adsorption mechanism, measurements of zero point charge (*pzc*) of the adsorbent are crucial, since it is well known that adsorption of a cation is favorable at pH > *pzc*. By contrast, for an anion the favorable adsorption condition is pH < *pzc*. Here we observed that the *pzc* of nanocomposite h-XG/SiO_2-2 is 3.6 (Figure 5a). Therefore, in an acidic environment (pH < *pzc*), a lower adsorption efficiency is expected because of the repulsive forces between the adsorbent and adsorbate. Additionally, in acidic pH, the increased surface excess of H^+ ions on the adsorbent implies competion of the H^+ ions with cationic dye molecules, which reduces the adsorption of dye molecules.[44] However, under alkaline conditions, the electrostatic attraction force increases, resulting in a higher % of adsorption of the cationic dye. This is attributed to an increase in the number of negatively charged sites, because of the deprotonation of carboxylic acid groups of the grafted chains. Further, the electrostatic repulsion among neighboring ionized groups is enhanced, resulting in an increase of the grafted chains inside the composite structure.[26,28] We conclude that the formation of ionic complexes between cationic dye (MB or MV) molecules and the anionic adsorbent is responsible for the high adsorption efficacy.

Effect of Contact Time. Figure 5c shows that the initial rate of dye uptake increased sharply with time and reached a maximum (99.4%) within 20 min for MB and within 15 min for MV (99.1%), after which it leveled off. This observation indicates that a monolayer of dye molecules at the external interface on the nanocomposite is formed. After the initially rapid adsorption, the dye adsorption rate was controlled by mass transport in the nanocomposite.[10,21]

Effect of Temperature. Figure 5d demonstrates the effect of temperature on the adsorption efficacy using the h-XG/SiO_2-2 nanocomposite. For MB, the adsorption efficacy was enhanced from 89.4% to 99.4% with a rise in temperature from 298 K to 323 K, beyond which it decreased to 93.5% at 333 K. By contrast, a maximum adsorption (99.1 %) was observed for MV at 313 K, which decreased to 91.9% with a further rise in temperature to 328 K. It is well known that adsorbate

dx.doi.org/10.1021/am4055657 | ACS Appl. Mater. Interfaces 2014, 6, 4766−4777

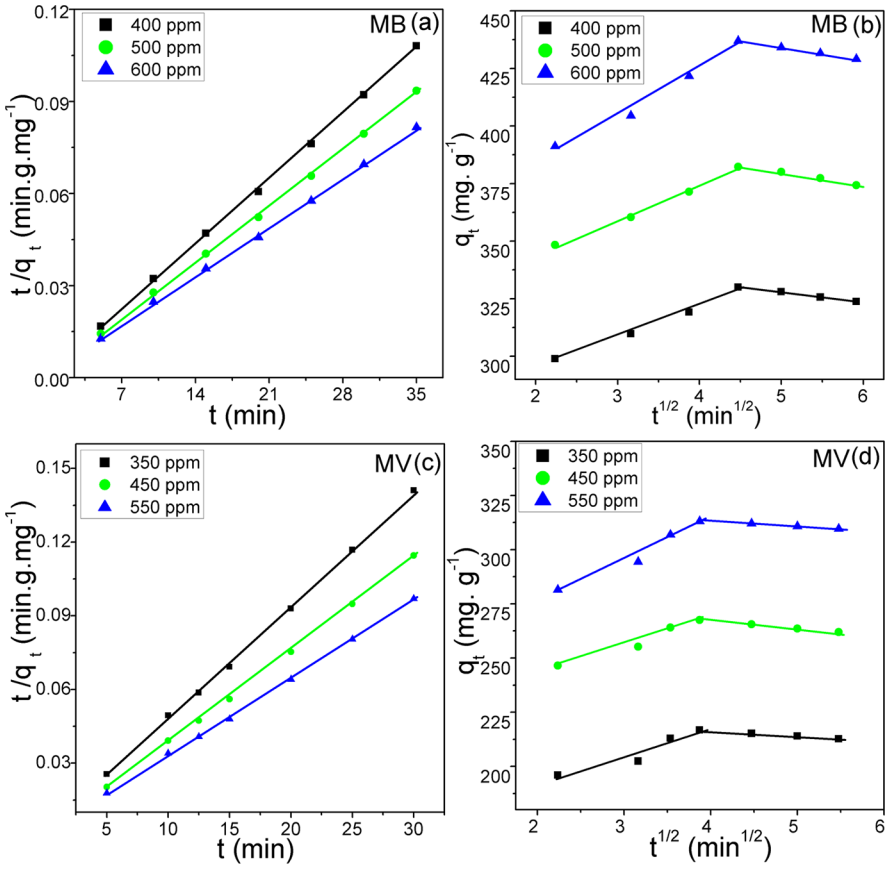

Figure 6. Modeling of the adsorption kinetics of MB using (a) pseudo-second-order and (b) intraparticle diffusion models, and MV using (c) pseudo-second-order and (d) intraparticle diffusion models onto h-XG/SiO_2-2 nanocomposite.

molecules, on contact with water, may or may not enter inside the adsorbate, which depends on the level of interaction between adsorbate and adsorbent.[21] In addition, at elevated temperatures, swelling may enable the passage of large dye molecules, which results in an increase in % adsorption.[21] Further, the increase in the adsorption rate with temperature may be because of the superior diffusion rate of the dye molecules as well as the lower solution viscosity of the adsorbent particles.[45] This confirms the endothermic nature of the dye uptake. However, at very high temperatures, desorption may take place because of enhanced thermal motions, which results in a lower % adsorption.[21]

Effect of Adsorbent Dosage. Figure 5e shows the effect of h-XG/SiO_2-2 nanocomposite dosage on the uptake of MB and MV from aqueous solution. The maximum color removal was found to be 99.4% at 30 mg adsorbent dosage for MB and 99.1 % at 40 mg nanocomposite dosage for MV, after which it reached a plateau. This phenomenon can be explained on the basis of higher surface area as well as increased availability of the active sites on the h-XG/SiO_2 nanocomposite surface. On the other hand, with higher adsorbent dosage, lower rate of adsorption have been witnessed due to the aggregation of adsorption sites and an enhanced diffusion path length, which caused a decrease of total available surface area.[46]

Effect of Dye Concentration. Figure 5f demonstrates the effect of the concentration of cationic dyes on the % adsorption using nanocomposite h-XG/SiO_2-2 as an adsorbent. It is obvious that the dye removal declined from 99.4% to 81.6% with an increase in MB concentration from 400 to 700 ppm, and in the case of MV, the dye adsorption decreased from 99.1% to 87.7% with increasing MV concentration from 350 to 650 ppm. This trend may be explained by the fact that at lower concentrations, a maximum number of dye molecules would be able to adsorb on h-XG/SiO_2-2 surface, ensuing a higher % of adsorption. By contrast, at higher dye concentrations, a lower % adsorption has been monitored due to the saturation of the active adsorption sites.[6,47]

Therefore, the optimized conditions for the maximum specific removal (Q_{max} = 497.5 mg g^{-1}) of MB are: pH 8; time 20 min; temperature 323 K; adsorbent dosage 30 mg/25 mL; initial dye concentration 400 ppm; and for MV (Q_{max} = 378.8 mg g^{-1}), the optimized adsorption parameters are pH 9; time 15 min; temperature 313 K; adsorbent dosage 40 mg/25 mL; initial dye concentration 350 ppm.

3.3.2. Effect of Ionic Strength. The effect of ionic strength on the adsorption efficiency of MB and MV on h-XG/SiO_2-2 nanocomposite was investigated. The results are shown in Figure S7 (see the Supporting Information). In the present study, NaCl and $CaCl_2$ solutions with concentration from 0.1 (M) to 0.6 (M) were utilized at otherwise constant parameters (pH 7, contact time 20 min, temperature 323 K, adsorbent dosage 30 mg/25 mL, dye concentration 400 ppm for MB and pH 7, contact time 15 min, temperature 313 K, adsorbent dosage 40 mg/25 mL, dye concentration 350 ppm for MV). The results (see Figure S7 in the Supporting Information) reveal that the color removal rate of the adsorbent gradually declined with an increase in ionic strength of both salts. This observation can be rationalized by considering the competitive effect between salt cations (Na^+ and Ca^{2+}) and hydrated cationic dye molecules with the negatively charged surface of

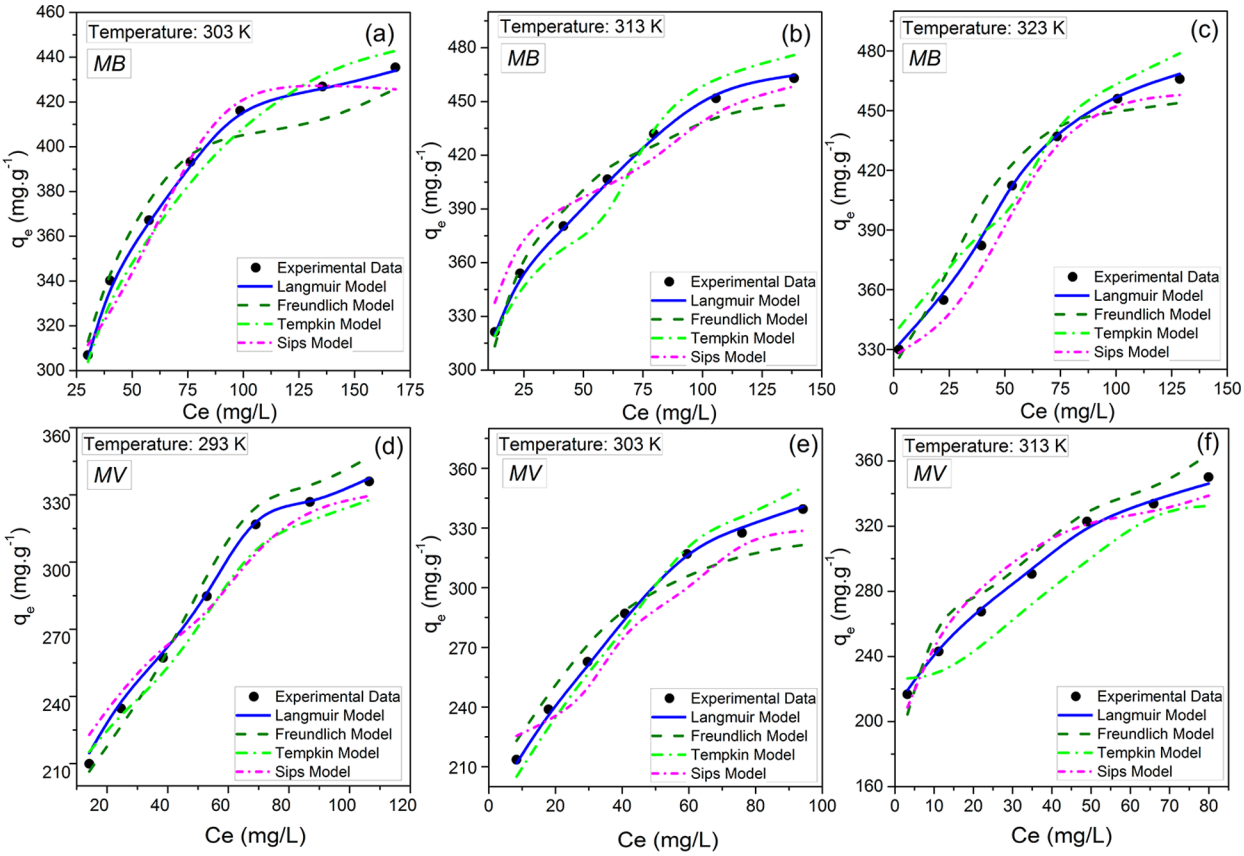

Figure 7. Various adsorption isotherm models fittedto the experimental data for the adsorption of MB at temperatures of (a) 303, (b) 313 (c) 323 K and the adsorption of MV at temperaturesof (d) 293, (e) 303, and (f) 313 K using the h-XG/SiO_2-2 nanocomposite.

the h-XG/SiO_2-2 nanocomposite. Similar observations were reported for the removal of MB using Cu^{2+} exchanged montmorillonite.[48] With an increase in salt concentration, the "ionic atmosphere" may also progressively enhance the shielding of the charge of cationic dye molecules, which reduces the adsorption rate.[48] However, as Ca^{2+} creates a greater contribution to the ionic strength compared to Na^+, the adsorption efficiency of nanocomposite in presence of Ca^{2+} ions is lower than that of Na^+ at the same concentration. This result suggests that electrostatic attraction is predominating between the anionic adsorbent (i.e. the h-XG/SiO_2 nanocomposite) and the cationic dye molecules.

3.3.3. Adsorption Kinetics. The rate of dye uptake depends on the contact time of the solid and liquid as well as on diffusion processes.[26] During the adsorption process, adsorbate molecules migrate to the outer surface of the adsorbent, diffuse in the boundary layer and eventually from the particle surface into the internal sites via pore diffusion. Thus, to explore the adsorption kinetics and understand the mechanism of adsorption, pseudo-first-order,[49] pseudo-second-order,[50] second-order,[51] and intraparticle diffusion[52] kinetics models were studied (for details, see the Supporting Information). The fits of the experimental results (see Table S3 in the Supporting Information) show that the pseudo second order model possesses a higher R^2 and a lower χ^2 value, compared to the pseudo-first-order and second-order models. This indicates that the adsorption kinetics may be described as a pseudo-second-order model (Figure 6) and depends on the amount of solute adsorbed on the surface of adsorbent and the amount adsorbed at equilibrium.[6] The linear form of the pseudo-second order kinetic rate equation is expressed as[50]

$$\frac{t}{q_t} = \frac{1}{K_2 q_e^2} + \frac{t}{q_e} \tag{4}$$

where K_2 (g mg^{-1} min^{-1}) is the pseudo-second-order rate constant.

Figure 6a (for MB) and Figure 6c (for MV) show the plot of t/q_t vs. t and the parameters K_2, q_e, and the R^2 and χ^2 values are given in Table S3 in the Supporting Information. The intraparticle diffusion kinetics model of Weber and Morris[52] is presented in Figure 6b (for MB) and Figure 6d (for MV); the linear form of this equation is

$$q_t = K_4 t^{1/2} + C \tag{5}$$

where K_4 (mg g^{-1} $min^{-1/2}$) is the intraparticle diffusion rate constant[52] and C is the boundary layer thickness[52] and the parameters K_4, q_e and the R^2 and χ^2 values are given in Table S3 in the Supporting Information.

Plots of q_t vs. $t^{1/2}$ show at least two linear segments (Figure 6b, d). The first phase represents boundary layer diffusion due to the mass transfer from the dye solution to the outer surface of the nanocomposite. The second portion indicates a steady adsorption step, corresponding to intraparticle diffusion of dye molecules[53] throughout the porous surface of the nanocomposite.

In addition, if the plot of q_t vs. $t^{1/2}$ passes through the origin, then intraparticle diffusion plays a crucial role in the adsorption kinetics.[30] However, the plots possess an intercept (see Table

dx.doi.org/10.1021/am4055657 | ACS Appl. Mater. Interfaces 2014, 6, 4766−4777

S3 in the Supporting Information), which indicates the thickness of the boundary layer. Therefore, the presence of multilinearity and the boundary layer thickness suggests that some other mechanism may also contribute significant role in the dye uptake process in combination with intra particle diffusion model. Thus it is believed that surface adsorption along with intraparticle diffusion takes place concurrently.

3.3.4. Adsorption Isotherm. The adsorption isotherm (Figure 7) explains the distribution of dye molecules between the liquid and the solid phase, when the processes involved equilibrium. To reveal the interactive behavior between the adsorbent and adsorbate molecules, appropriate adsorption isotherm models, including the Langmuir,[54] Freundlich,[55] Temkin[56] and Sips isotherms,[57] were tested (for details, see the Supporting Information).The data were found to agree best with the Langmuir model (Figure 7), which assumes that adsorption took place on the homogeneous surface of adsorbent with identical binding sites and that no trans-migration between the adsorbed species occurs.[54] The nonlinear mathematical expression of the Langmuir model[54] is

$$q_e = \frac{bQ_0C_e}{1 + bC_e} \tag{6}$$

where C_e is the equilibrium concentration of adsorbate (mg L^{-1}), q_e is the amount of dye adsorbed by the nanocomposite at equilibrium (mg g^{-1}), Q_0 (mg g^{-1}) signifies the maximum adsorption capacity and the Langmuir constant b (L mg^{-1})-relates to free energy and affinity of adsorption.[37,54] The feasibility of the adsorption process is calculated using separation factor (R_L),[6] which is defined by following equation

$$R_L = \frac{1}{1 + bC_0} \tag{7}$$

The value of R_L indicates the category of the isotherm to be either unfavorable ($R_L > 1$), linear ($R_L = 1$), irreversible ($R_L = 0$) or favorable ($0 < R_L < 1$).[6]

It is evident from Figure 7 that the Langmuir isotherm model shows a better fit with the experimental data in comparison to the other models studied here. The Freundlich constant increased with rise in temperature, suggesting the process is endothermic. The Langmuir constant "*b*" increased with temperature, which represents the stronger attraction between the active sites of the adsorbent and adsorbate,[21] and also indicates a higher affinity of adsorbent and adsorbate molecules at higher temperature in comparison to lower temperature.[21] At an MB concentration of 400 mg L^{-1}, R_L was calculated to be 0.0179 at 323 K and in the case of 350 mg L^{-1} the value of R_L was observed as 0.0179 at 313 K for MV. This observation further supports that the Langmuir adsorption isotherm is favorable. Finally, Q_{max} was calculated for both dyes and found to be 497.5 mg g^{-1} at 323 K for MB and 378.8 mg g^{-1} at 313 K for MV, respectively (see Table S4 in the Supporting Information). This result suggests that the h-XG/SiO_2-2 nanocomposite possesses a high capability to remove both cationic dyes from aqueous solution.

3.3.5. Adsorption Thermodynamics. The van't Hoff analysis was used to unveil the spontaneity of the adsorption of MB and MV on the h-XG/SiO_2 nanocomposites and to afford various thermodynamic parameters.

$$\ln b = \frac{\Delta S^\circ}{R} - \frac{\Delta H^\circ}{RT} \tag{8}$$

$$\Delta G^\circ = \Delta H^\circ - T\Delta S^\circ \tag{9}$$

where ΔG° is the change in Gibbs free energy (J. mol^{-1}), ΔH° is change in enthalpy (J. mol^{-1}), ΔS° is the change in entropy (J. mol^{-1} K^{-1}), R is universal gas constant (8.314 J. K^{-1} mol^{-1}) and b is Langmuir constant at temperature T (K).

The values of ΔS° and ΔH° were evaluated from the intercept and slope of a plot of *ln b* vs. *1/T* (Figure S9, Supporting Information); the parameters are reported in Table S5 (Supporting Information). The negative values of ΔG° confirm the spontaneous nature of the dye uptake process. It was also observed that the ΔG° values gradually decreased with increasing temperature. The positive values of ΔH° suggest that the process is endothermic[10] and the positive values of ΔS° reveal the increase in randomness at the solid-solution interface all through the adsorption of MB and MV dyes on the active sites of adsorbent.[14,21]

3.3.6. Comparison of the Adsorption Capacity with Various Adsorbents. To investigate the efficiency of the h-XG/SiO_2-2 nanocomposite as adsorbent for uptake of MB and MV from aqueous solution, the Q_{max} of the h-XG/SiO_2-2 was compared with various reported adsorbent. Although it is complicated to directly compare the adsorption efficacy of the h-XG/SiO_2 with literature data due to the dissimilar experimental conditions, Table S6 (Supporting Information) reveals that the adsorption capacity of h-XG/SiO_2-2 (497.5 mg g^{-1} for MB and 378.8 mg g^{-1} for MV) is better than that of various reported adsorbents used for removal of MB and MV.[2,3,6−8,13,15,17,26,28−37]This result suggests that h-XG/SiO_2 nanocomposites can be considered as promising adsorbents for the removal of MB and MV from aqueous solution.

3.3.7. Regeneration Study. The adsorption and desorption characteristics of an adsorbent is very important for its potential application. An efficient adsorbent should possess both high adsorption capacities as well as excellent desorption characteristics, to render the sorbent economically viable. Therefore, to explicate the mechanism of sorption, desorption experiments were performed with different media of *pH* 2, 7, and 10. For these three solutions, the maximum % desorption was achieved in *pH* 2 (95.7% for MB and 95.5 % for MV) and the minimum % desorption was observed at *pH* 10 (51.3% for MB and 49.9% for MV), which is the opposite trend compared to the adsorption process. This result signifies that ion exchange may be the key adsorption mechanism. The probable desorption mechanism is represented in Scheme S1 (Supporting Information). Hence to realize the regeneration efficacy of h-XG/SiO_2-2, adsorption-desorption cycles were carried out in concert for four times at *pH* 2. It was found that 85.6 % of MB and 83.5 % of MV were desorbed after the 4th cycle (Figure S10, Supporting Information). Thus, it can be concluded that the h-XG/SiO_2-2 nanocomposite showed excellent recycling ability for the treatment of the MB and MV from aqueous solution.

3.3.8. Adsorption Mechanism. It is well known that various factors including functional behavior and structure of adsorbate molecules, surface of the adsorbent along with interaction among adsorbent and adsorbate influence the dye adsorption mechanism.[21] Figure S11 (Supporting Information) shows that the h-XG/SiO_2 nanocomposites exhibit better dye adsorption characteristics in comparison with h-XGs under optimized adsorption conditions. This result is attributed to the enhanced hydrodynamic volume, high surface area as well as the existence of additional chelating binding sites on the nanocomposite

surface. Further, compared to the other nanocomposites, h-XG/SiO_2-2 showed higher dye removal efficiency, probably because of the uniform distribution of nanofillers throughout the polymer matrix, which enhanced the H-bonding interaction between silica and modified polysaccharide matrix.

The FTIR spectra of the h-XG/SiO_2-2 nanocomposite (Figure S12a, Supporting Information), nanocomposite with adsorbed MB (Figure S12c, Supporting Information) and adsorbed MV (Figure S12e, Supporting Information) suggest the possible interaction sites between adsorbent and adsorbate molecule. In the spectra characteristic peak shifts were observed. After adsorption, the characteristics peaks for the dye loaded h-XG/SiO_2-2 nanocomposite shifted e.g. for silanol−OH stretching from 3787 cm^{-1} to 3779 cm^{-1} (for MB) and to 3770 cm^{-1} (for MV), −OH stretching vibration from 3460 cm^{-1} to 3427 cm^{-1} (for MB) and to 3436 cm^{-1} (for MV), COO^- symmetric stretching vibrations from 1456 cm^{-1} to 1439 cm^{-1} (for MB) and to 1440 cm^{-1} (for MV), COO^- asymmetric stretching vibrations from 1562 cm^{-1} to 1553 cm^{-1} (for MB) and to 1548 cm^{-1} (for MV), and for amide − I, the shift took place from 1669 cm^{-1} to 1660 cm^{-1} (for MB) and to 1659 cm^{-1} (for MV). However, there is no significant change took place for peak corresponding to C−H stretching (2939 cm^{-1}) and C−N stretching vibrations (1399 cm^{-1}). This indicates the specific electrostatic as well as H-bonding interaction between the active sites of cationic MB and MV dyes and the silanol − OH as well as polysaccharide −OH groups, amide carbonyl groups and $-COO^-$ groups of nanocomposite, as shown in Scheme 2.

Scheme 2. Adsorption Mechanism of (a) MB and (b) MV Using h-XG/SiO_2-2 Nanocomposites

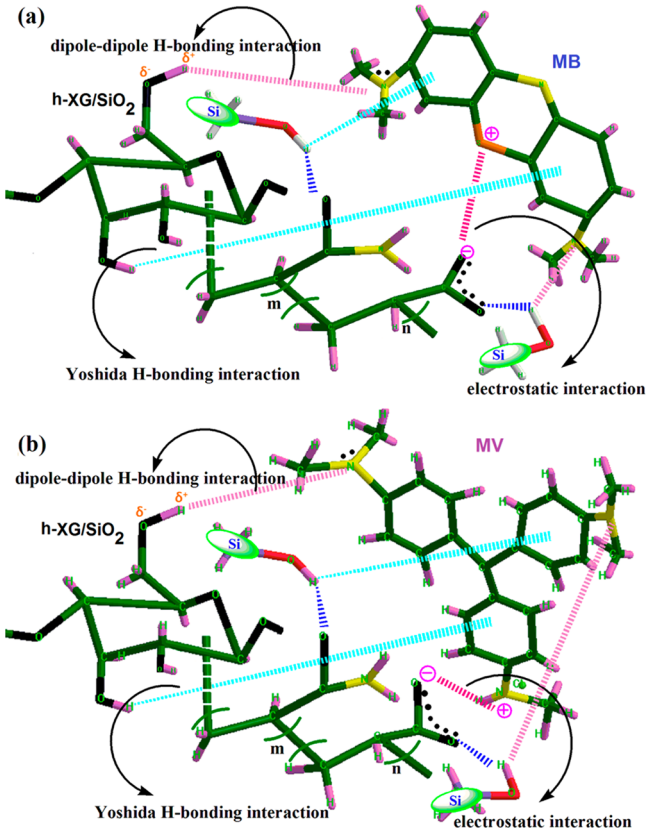

FE-SEM measurements were also carried out to compare the morphological features and surface characteristics of h-XG/SiO_2-2 adsorbent after adsorption of MB (Figure S13a, Supporting Information) and MV (Figure S13b, Supporting Information). The appearance of layers (with bright contrast in the secondary electron images) is evidenced from FE-SEM images for both dyes, which is due to the significant accumulation of MB and MV over the adsorbent surface[3] owing to the physical interaction among the adsorbate and adsorbent molecules. Further, the salt effect study revealed that the adsorption efficacy decrease with increasing ionic strength, which confirms the existence of electrostatic interaction between cationic dye molecules and anionic adsorbent. The efficient regeneration property of the h-XG/SiO_2 nanocomposite implies that ion exchange might be a probable mechanism for the adsorption process of the cationic dyes. Thus it is presumed that the possible interaction involved in MB and MV uptake process is the electrostatic interaction between COO^- groups of adsorbent and the positively charged active sites of the dye molecule as well as dipole−dipole H-bonding interaction between the several −OH groups present on the adsorbent surface and the electronegative residue (N lone pair) in the dye molecule.[13] Additionally, Yoshida H-bonding interaction between silanol −OH groups, large number of −OH groups present in polysaccharides and the active sites of cationic dyes (aromatic ring) plays a crucial role in adsorption phenomenon.[58]

The adsorption mechanism can also be explained by consecutive process of dye diffusion comprising bulk diffusion, intraparticle diffusion and surface adsorption.[2] It was found that the removal of MB and MV is initially rapid and subsequently equilibrium is reached more slowly. This confirms that initially a rapid dye uptake has occurred through a surface adsorption process. The hydrophilic nature of the adsorbent is mainly responsible for a fast adsorption due to surface mass transport. However, the entangled chains of the polymeric nanocomposite network facilitate the diffusion process as the carboxylate groups are hydrophilic in nature and are expected to swell in aqueous media allowing the fast diffusion of dyes. Thus the intraparticle diffusion process might also take place for the adsorption process of cationic dyes and may control the adsorption mechanism. The Langmuir isotherm may also hint at the homogeneous nature of the h-XG/SiO_2 nanocomposite surface with equal identical binding sites and monolayer coverage of dyes. Finally, the negative ΔG° value reveals that the adsorption process is spontaneous in nature.

We have additionally investigated the uptake capacity of the anionic dye Congo red (CR) from aqueous solution using the h-XG/SiO_2-2 nanocomposite. The details of optimized parameters of CR adsorption efficacy are explained in Figure S14 (Supporting Information). It was found that only 63.1 mg g^{-1} CR dye was removed after prolonged adsorption for 150 min. Because of the anionic nature of the dye it is assumed that only H-bonding interaction is taking place between the different organic functional groups present in the adsorbate and adsorbent as evidenced from FTIR spectra (Figure S15, Supporting Information). This also opens up the perspective that this novel nanocomposite (i.e. h-XG/SiO_2-2) may act as a competent adsorbent for selective adsorption of cationic dyes.

4. CONCLUSIONS

It can be concluded that the in situ incorporation of silica nanoparticles on h-XG affords a high performance, novel

dx.doi.org/10.1021/am4055657 | ACS Appl. Mater. Interfaces 2014, 6, 4766−4777

nanocomposite-based adsorbent, which shows excellent cationic dye removal efficacy from aqueous solution. This dye uptake efficacy of the nanocomposite is attributed to its high hydrodynamic volume and high specific surface area, which originates from the uniform distribution of SiO_2 nanoparticles in the polymer matrix of partially hydrolyzed polyacrylamide grafted onto xanthan gum. The adsorption capacity of h-XG/SiO_2-2 is considerably higher in contrast to various reported adsorbents used for cationic dye removal and also showed good recyclability. Thus, h-XG/SiO_2 based nanocomposites might be promising adsorbents for selective removal of cationic dye pollutants from aqueous solution.

■ ASSOCIATED CONTENT

Supporting Information

The results of elemental analyses (Table S1), table of ^{13}C and ^{29}Si NMR data (Table S2), details of various models of adsorption kinetics and adsorption isotherm, tables of adsorption kinetics (Table S3), adsorption isotherms (Table S4), adsorption thermodynamics (Table S5), a comparative table of adsorption capacity vs. other reported adsorbents (Table S6), ^{29}Si MAS-NMR spectra (Figure S1), EDAX analysis of h-XG 7 and various nanocomposites (Figure S2), TEM data of h-XG/SiO_2-1 and h-XG/SiO_2-3 nanocomposites (Figure S3), TEM analysis of Stöber silica (Figure S4), nitrogen adsorption-desorption isotherms (Figure S5), rheological characteristics (Figure S6), data on the effect of salt concentration on the adsorption efficacy (Figure S7), modelling of adsorption kinetics of MB and MV using pseudo-first-order and second order models onto h-XG/SiO_2-2 (Figure S8), thermodynamic parameters for adsorption of MB and MV using the h-XG/SiO_2-2 (Figure S9), simultaneous adsorption-desorption cycles (Figure S10), comparison of MB and MV removal capacity of various h-XGs and nanocomposites (Figure S11), FTIR spectra of the nanocomposite and MB and MV dye-loaded nanocomposite (Figure S12), FE-SEM analyses of MB and MV dye loaded nanocomposites (Figure S13), optimized parameters for Congo red dye uptake study (Figure S14), FTIR spectra of CR dye and CR dye loaded nanocomposite (Figure S15), and details of the desorption mechanism (Scheme S1). This material is available free of charge via the Internet at http://pubs.acs.org.

■ AUTHOR INFORMATION

Corresponding Authors

*E-mail: abpanda@csmcri.org. Tel: +91-278-2567760, ext. 704 .

*E-mail: schoenherr@chemie.uni-siegen.de. Tel: +49-271-7402806. Fax: +49-271-7402805.

*E-mail: sagarpal1@hotmail.com. Tel: +91-326-2235769. Fax: 0091-326-2296615.

Notes

The authors declare no competing financial interest.

■ ACKNOWLEDGMENTS

The authors are indebted to Prof. X. Jiang (LOT, University of Siegen) for access to the FE-SEM and gratefully acknowledge financial support from Department of Science and Technology, New Delhi, India in form of a research grant (DST/TSG/WP/69/2009) to carry out the reported investigation as well as partial financial support by the German Academic Exchange Service (DAAD, stipend to SP in the frame work of the "Program for Research Visits"), the European Research Council (ERC grant to HS, ERC grant agreement 279202), the Indian School of Mines, Dhanbad and the University of Siegen.

■ REFERENCES

(1) Madadrang, C. J.; Kim, H. Y.; Gao, G.; Wang, N.; Zhu, J.; Feng, H.; Gorring, M.; Kasner, M. L.; Hou, S. Adsorption Behavior of EDTA-Graphene Oxide for Pb (II) Removal. *ACS Appl. Mater. Interfaces* **2012**, *4*, 1186−1193.

(2) Liu, F.; Chung, S.; Oh, G.; Seo, T. S. Three-Dimensional Graphene Oxide Nanostructure for Fast and Efficient Water-Soluble Dye Removal. *ACS Appl. Mater. Interfaces* **2012**, *4*, 922−927.

(3) Ma, J.; Yu, F.; Zhou, L.; Jin, L.; Yang, M.; Luan, J.; Tang, Y.; Fan, H.; Yuan, Z.; Chen, J. Enhanced Adsorptive Removal of Methyl Orange and Methylene Blue from Aqueous Solution by Alkali-Activated Multiwalled Carbon Nanotubes. *ACS Appl. Mater. Interfaces* **2012**, *4*, 5749−5760.

(4) Gupta, V. K.; Ali, I. Removal of Endosulfan and Methoxychlor from Water on Carbon Slurry. *Environ. Sci. Technol.* **2008**, *42*, 766−770.

(5) Cai, T.; Yang, Z.; Li, H.; Yang, Hu.; Li, A.; Cheng, R. Effect of Hydrolysis Degree of Hydrolyzed Polyacrylamide Grafted Carboxymethyl Cellulose on Dye Removal Efficiency. *Cellulose* **2013**, *20*, 2605−2614.

(6) Ayad, M. M.; El-Nasr, A. A. Adsorption of Cationic Dye (Methylene Blue) from Water Using Polyaniline Nanotubes Base. *J. Phys. Chem. C* **2010**, *114*, 14377−14383.

(7) Xu, R. K.; Xiao, S. C.; Yuan, J. H.; Zhao, A. Z. Adsorption of Methyl Violet from Aqueous Solutions by the Biochars Derived from Crop Residues. *Bioresour. Technol.* **2011**, *102*, 10293−10298.

(8) Hameed, B. H. Equilibrium and Kinetic Studies of Methyl Violet Sorption by Agricultural Waste. *J. Hazard. Mater.* **2008**, *154*, 204−212.

(9) Zhuang, X.; Wan, Y.; Feng, C.; Shen, Y.; Zhao, D. Highly Efficient Adsorption of Bulky Dye Molecules in Wastewater on Ordered Mesoporous Carbons. *Chem. Mater.* **2009**, *21*, 706−716.

(10) Rahchamani, J.; Mousavi, H. Z.; Behzad, M. Adsorption of Methyl Violet from Aqueous Solution by Polyacrylamide as an Adsorbent: Isotherm and Kinetic Studies. *Desalination* **2011**, *267*, 256−260.

(11) Cheng, R.; Ou, S.; Xiang, B.; Li, Y.; Liao, Q. Equilibrium and Molecular Mechanism of Anionic Dyes Adsorption onto Copper (II) Complex of Dithiocarbamate-Modified Starch. *Langmuir* **2010**, *26*, 752−758.

(12) Song, S.; Feng, L.; Song, A.; Hao, J. Room-Temperature Super Hydrogel as Dye Adsorption Agent. *J. Phys. Chem. B* **2012**, *116*, 12850−12856.

(13) Parker, H. L.; Hunt, A. J.; Budarin, V. L.; Shuttleworth, P. S.; Miller, K. L.; Clark, J. H. The Importance of Being Porous: Polysaccharide-Derived Mesoporous Materials for Use in Dye Adsorption. *RSC Adv.* **2012**, *2*, 8992−8997.

(14) Zhou, Y.; Zhang, M.; Hu, X.; Wang, X.; Niu, J.; Ma, T. Adsorption of Cationic Dyes on a Cellulose-Based Multicarboxyl Adsorbent. *J. Chem. Eng. Data* **2013**, *58*, 413−421.

(15) Zhang, W.; Yang, H.; Dong, L.; Yan, H.; Li, H.; Jiang, Z.; Kan, X.; Li, A.; Cheng, R. Efficient Removal of Both Cationic and Anionic Dyes from Aqueous Solutions using a Novel Amphoteric Straw-based Adsorbent. *Carbohydr. Polym.* **2012**, *90*, 887−893.

(16) Singh, V.; Sharma, A. K.; Sanghi, R. Poly(acrylamide) Functionalized Chitosan: An Efficient Adsorbent for Azo Dyes from Aqueous Solutions. *J. Hazard. Mater.* **2009**, *166*, 327−335.

(17) Dou, X.; Li, P.; Zhang, Di.; Feng, C. L. C_2-Symmetric Benzene-based Hydrogels with Unique Layered Structures for Controllable Organic Dye Adsorption. *Soft Matter* **2012**, *8*, 3231−3238.

(18) Travlou, N. A.; Kyzas, G. Z.; Lazaridis, N. K.; Deliyanni, E. A. Functionalization of Graphite Oxide with Magnetic Chitosan for the Preparation of a Nanocomposite Dye Adsorbent. *Langmuir* **2013**, *29*, 1657−1668.

(19) Zhao, G.; Li, J.; Ren, X.; Chen, C.; Wang, X. Few-Layered Graphene Oxide Nanosheets as Superior Sorbents for Heavy Metal Ion Pollution Management. *Environ. Sci. Technol.* **2011**, *45*, 10454−10462.
(20) Pandey, S.; Mishra, S. B. Sol−gel Derived Organic−Inorganic Hybrid Materials: Synthesis, Characterizations and Applications. *J. Sol−Gel Sci. Technol.* **2011**, *59*, 73−94.
(21) Ghorai, S.; Sarkar, A. K.; Panda, A. B.; Pal, S. Effective Removal of Congo Red Dye from Aqueous Solution using Modified Xanthan Gum/Silica Hybrid Nanocomposite as Adsorbent. *Bioresour. Technol.* **2013**, *144*, 485−491.
(22) Singh, V.; Tiwari, A.; Pandey, S.; Singh, S. K.; Sanghi, R. Synthesis and Characterization of Novel Saponified Guar-Graft-Poly(acrylonitrile)/Silica Nanocomposite Materials. *J. Appl. Polym. Sci.* **2007**, *104*, 536−544.
(23) Shchipunov, Y. A.; Karpenko, T. Y. Hybrid Polysaccharide-Silica Nanocomposites Prepared by the Sol-Gel Technique. *Langmuir* **2004**, *20*, 3882−3887.
(24) Ghorai, S.; Sinhamahpatra, A.; Sarkar, A.; Panda, A. B.; Pal, S. Novel Biodegradable Nanocomposite based on XG-g-PAM/SiO_2: Application of an Efficient Adsorbent for Pb^{2+} Ions from Aqueous Solution. *Bioresour. Technol.* **2012**, *119*, 181−190.
(25) Singh, V.; Pandey, S.; Singh, S. K.; Sanghi, R. Removal of Cadmium from Aqueous Solutions by Adsorption using Poly-(acrylamide) Modified Guar Gum−Silica Nanocomposites. *Sep. Purif. Technol.* **2009**, *67*, 251−261.
(26) Pal, S.; Ghorai, S.; Das, C.; Samrat, S.; Ghosh, A.; Panda, A. B. Carboxymethyl Tamarind-g-Poly (Acrylamide)/Silica: A High Performance Hybrid Nanocomposite for Adsorption of Methylene Blue Dye. *Ind. Eng. Chem. Res.* **2012**, *51*, 15546−15556.
(27) Ghorai, S.; Sarkar, A.; Panda, A. B.; Pal, S. Evaluation of the Flocculation Characteristics of Polyacrylamide Grafted Xanthan Gum/Silica Hybrid Nanocomposite. *Ind. Eng. Chem. Res.* **2013**, *52*, 9731−9740.
(28) Paulino, A. T.; Guilherme, M. R.; Reis, A. V.; Campese, G. M.; Muniz, E. C.; Nozaki, J. Removal of Methylene Blue Dye from an Aqueous Media Using Superabsorbent Hydrogel Supported on Modified Polysaccharide. *J. Colloid Interface Sci.* **2006**, *301*, 55−62.
(29) Tang, Y. T.; Dou, X. Q.; Ji, Z. A.; Li, P.; Zhu, S. M.; Gu, J. J.; Feng, C. L.; Zhang, D. C_2-Symmetric Cyclohexane-Based Hydrogels: A Rational Designed LMWG and its Application in Dye Scavenging. *J. Mol. Liq.* **2013**, *177*, 167−171.
(30) Ai, L.; Li, M.; Li, L. Adsorption of Methylene Blue from Aqueous Solution with Activated Carbon/Cobalt Ferrite/Alginate Composite Beads: Kinetics, Isotherms, and Thermodynamics. *J. Chem. Eng. Data* **2011**, *56*, 3475−3483.
(31) Liu, R.; Zhang, B.; Mei, D.; Zhang, H.; Liu, J. Adsorption of Methyl Violet from Aqueous Solution by Halloysite Nanotubes. *Desalination* **2011**, *268*, 111−116.
(32) Azizian, S.; Haerifar, M.; Bashiri, H. Adsorption of Methyl Violet onto Granular Activated Carbon: Equilibrium, Kinetics and Modeling. *Chem. Eng. J.* **2009**, *146*, 36−41.
(33) Duran, C.; Ozdes, D.; Gundogdu, A.; Senturk, H. B. Kinetics and Isotherm Analysis of Basic Dyes Adsorption onto Almond Shell (Prunus Dulcis) as a Low Cost Adsorbent. *J. Chem. Eng. Data* **2011**, *56*, 2136−2147.
(34) Mall, I. D.; Srivastava, V. C.; Agarwal, N. K. Removal of Orange-G and Methyl Violet Dyes by Adsorption onto Bagasse Fly Ash-Kinetic Study and Equilibrium Isotherm Analyses. *Dyes Pigm.* **2006**, *69*, 210−223.
(35) Xu, S.; Wang, J.; Wu, R.; Wang, J.; Li, H. Adsorption Behaviors of Acid and Basic Dyes on Crosslinked Amphoteric Starch. *Chem. Eng. J.* **2006**, *117*, 161−167.
(36) Ho, Y. S.; Chiu, W. T.; Wang, C. C. Regression Analysis for the Sorption Isotherms of Basic Dyes on Sugarcane Dust. *Bioresour. Technol.* **2005**, *96*, 1285−1291.
(37) Tian, Y.; Ji, C.; Zhao, M.; Xu, M.; Zhang, Y.; Wang, R. Preparation and Characterization of Baker's Yeast Modified by Nano-Fe_3O_4: Application of Biosorption of Methyl Violet in Aqueous Solution. *Chem. Eng. J.* **2010**, *165*, 474−481.
(38) Krishnamoorthi, S.; Singh, R. P. Synthesis, Characterization, Flocculation and Rheological Characteristics of Hydrolyzed and Unhydrolyzed Polyacrylamide-Grafted Poly(Vinyl Alcohol). *J. Appl. Polym. Sci.* **2006**, *101*, 2109−2122.
(39) Tripathy, T.; Singh, R. P. High Performance Flocculating Agent Based on Partially Hydrolyzed Sodium Alginate-g-Polyacrylamide. *Eur. Polym. J.* **2000**, *36*, 1471−1476.
(40) Sajab, M. S.; Chia, C. H.; Zakaria, S.; Jani, S. M.; Ayob, M. K.; Chee, K. L.; Khiew, P. S.; Chiu, W. S. Citric Acid Modified Kenaf Core Fibres for Removal of Methylene Blue from Aqueous Solution. *Bioresour. Technol.* **2011**, *102*, 7237−7243.
(41) Khalil, M. I.; Farag, S.; Fattach, S. A. E. Hydrolysis of Poly(acry1amide)-Starch Graft Copolymer. *J. Appl. Polym. Sci.* **1995**, *57*, 335−342.
(42) Gao, L.; Sun, J.; Zhang, L.; Wang, J.; Ren, B. Influence of Different Structured Channels of Mesoporous Silicate on the Controlled Ibuprofen Delivery. *Mater. Chem. Phys.* **2012**, *135*, 786−797.
(43) Copello, G. J.; Mebert, A. M.; Raineri, M.; Pesenti, M. P.; Diaz, L. E. Removal of Dyes from Water Using Chitosan Hydrogel/SiO_2 and Chitin Hydrogel/SiO_2 Hybrid Materials Obtained by the Sol−Gel method. *J. Hazard. Mater.* **2011**, *186*, 932−939.
(44) Crini, G.; Peindy, H. N.; Gimbert, F.; Robert, C. Removal of CI Basic Green 4 (Malachite Green) from Aqueous Solutions by Adsorption using Cyclodextrin-Based Adsorbent: Kinetic and Equilibrium Studies. *Sep. Purif. Technol.* **2007**, *53*, 97−110.
(45) Chowdhury, S.; Mishra, R.; Saha, P.; Kushwaha, P. Adsorption Thermodynamics, Kinetics and Isosteric Heat of Adsorption of Malachite Green onto Chemically Modified Rice Husk. *Desalination* **2011**, *265*, 159−168.
(46) Garg, V. K.; Kumar, R.; Gupta, R. Removal of Malachite Green Dye from Aqueous Solution by Adsorption using Agro-Industry Waste: A Case Study of *Prosopis Cineraria*. *Dyes Pigm.* **2004**, *62*, 1−10.
(47) Mahmoodi, N. M. Equilibrium, Kinetics, and Thermodynamics of Dye Removal using Alginate in Binary Systems. *J. Chem. Eng. Data* **2011**, *56*, 2802−2811.
(48) Ma, Y. L.; Xu, Z. R.; Guo, T.; You, P. Adsorption of Methylene Blue on Cu(II)-Exchanged Montmorillonite. *J. Colloid Interface Sci.* **2004**, *280*, 283−288.
(49) Legergren, S. About the Theory of so-Called Adsorption of Soluble Substances. *K. Sven. Vetenskapsakad. Handl.* **1898**, *Band 24*, 1−39.
(50) Ho, Y. S.; McKay, G. Pseudo-Second Order Model for Sorption Processes. *Process Biochem.* **1999**, *34*, 451−465.
(51) Ho, Y. S. Second-Order Kinetic Model for the Sorption of Cadmium onto Tree Fern: A Comparison of Linear and Non-linear Methods. *Water Res.* **2006**, *40*, 119−125.
(52) Weber, W. J.; Morris, J. C. Kinetics of Adsorption on Carbon from Solution. *J. San. Eng. Div. ASCE* **1963**, *89*, 31−59.
(53) Ai, L.; Zhang, C.; Meng, L. Adsorption of Methyl Orange from Aqueous Solution on Hydrothermal Synthesized Mg-Al Layered Double Hydroxide. *J. Chem. Eng. Data.* **2011**, *56*, 4217−4225.
(54) Langmuir, I. The Constitution and Fundamental Properties of Solids and Liquids. *J. Am. Chem. Soc.* **1916**, *38*, 2221−2295.
(55) Freundlich, H. M. F. Über die Adsorption in Lösungen. *Z. Phys. Chem.* **1906**, *57*, 385−470.
(56) Temkin, M. J.; Pyzhev, V. Recent Modifications to Langmuir Isotherms. *Acta Physicochem.* **1940**, *12*, 217−222.
(57) Sips, R. Combined Form of Langmuir and Freundlich Equations. *J. Chem. Phys.* **1948**, *16*, 490−495.
(58) Blackburn, R. S. Natural Polysaccharides and Their Interactions with Dye Molecules: Applications in Effluent Treatment. *Environ. Sci. Technol.* **2004**, *38*, 4905−4909.